

# Oil & Natural Gas Technology

DOE Award No.: DE-FE0009904

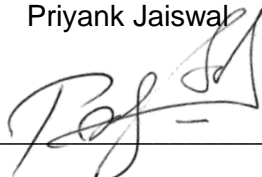
## Quarterly Research Performance Progress Report (Period ending 12/31/2015)

### Structural and Stratigraphic Controls on Methane Hydrate occurrence and distribution: Gulf of Mexico, Walker Ridge 313 and Green Canyon 955

Project Period: 10/01/2012 – 08/31/2016

Submitted by:

Priyank Jaiswal



Signature



Office of Fossil Energy



## Executive Summary

This quarterly progress summarizes the progress made towards the completion of Phase 3 which comprises rock physics modeling. In this report a rock physics model of Well H is presented. This model shows that the sand mass where Well H has high resistivity might actually comprise laminated sheets of coarse grained sediments. Logging-while-drilling (LWD) data from the Gulf of Mexico JIP Leg 2 drilling expedition in the Green Canyon 955 (GC955) block indicated high hydrate saturations in a sand-rich interval with no underlying free gas in Well H. Morphology of hydrates within sands in GC955 has remained poorly understood. Here, using the resistivity and compressional wave velocity logs, we estimate hydrate saturation and present a possible rock model of the hydrate-bearing sands in Well H. Additional presence of dipole log (Shear-wave velocity) would have been extremely helpful. In its absence the current model satisfies all observation.

Two observations drive our model building: a) Correlation between hydrate presence and borehole size, which we interpret as hydrate bonding the sediment grains and enhancing their mechanical stability which in turn prevents borehole enlargement; and b) Discrepancy in hydrate saturations from the ring resistivity and the propagation resistivity using Archie's method, which we interpret as due to presence of thin beds. Ring resistivity, which has the finest vertical resolution, is consistent with a laminated model which envisions hydrate-saturated sediment lenses embedded in hydrate-free background. The laminated model is also able to reproduce the measured compressional velocity. Results suggests a maximum hydrate saturation of 30% with a gross-to-net reservoir ratio of 20%. We conclude significant compartmentalization within the GC955H sands.

## Background

The overall objective is to identify and understand structural and stratigraphic controls on hydrate accumulation and distribution in leased blocks WR313 (WR: Walker Ridge) and GC955 (GC: Green Canyon) in the Gulf of Mexico using seismic and well data (Figure 1). The effort is to be completed in three phases. In the first phase, the objective is to create a large-scale (resolution in the order of Fresnel zone) P-wave velocity model using traveltime inversion and a corresponding depth image using pre-stack depth migration (PSDM). This phase was completed in due time. In the second phase, the objective was to jointly interpret the pre-stack depth migrated images and the full-waveform  $V_p$  models that were obtained as Phase 1 and Phase 2 deliverables. This phase was also completed in due time and a manuscript summarizing the efforts up till Phase 2 for GC955 was communicated to Journal of

Geophysical Research – Solid Earth. The papers are currently under revisions. The WR313 datasets did not give good results and therefore a no-cost extension has been sought. The third phase has two objectives. The first objective is to create a hydrate distribution map with the help of P-wave velocity and attenuation model created in the second phase and rock physics modeling. This report describes the progress made towards rock physics modeling of Well H logs from GC955.

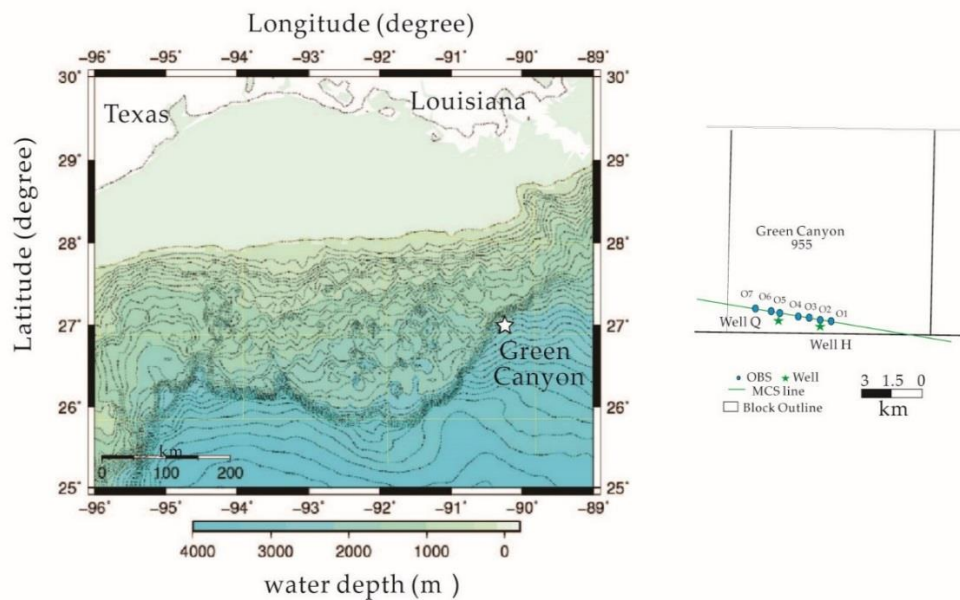


Figure 1: Base map. Seafloor bathymetry of Gulf of Mexico showing the location of the study area at the mouth of Green Canyon. The acquisition layout within lease block Green Canyon 955 (GC955) is shown in the inset. Solid line is the track of the multi-channel seismic (MCS) profile. Solid circles are location of ocean bottom seismometers (OBS) O1 – O7. Solid stars mark the locations of the wells Q and H that were drilling during the Joint Industry Project Leg II (JIP II).

We have developed a rock physics model for understanding the hydrate morphology in course-grained sediment sample by Well H in GC955. The GC955 lease block lies in the GOM abyssal plain outboard of the Sigsbee Escarpment, approximately 310 km south of New Orleans with water depth varying 2000-2200 m (Figure 1). Well H was drilled on a four-way structural closure within the hydrate stability zone and logged using LWD methods. High resistivity was observed at both fine-grained and course-grained units (lithology of these units have been previously inferred by Collett et al., 2012) which was considered as indicative of presence of hydrate. Here we are focusing only on the course-grained interval as it is most relevant to hydrate production.

## Approach

A rock physics model is a set of first-principle based mathematical equations that describe relationship between a rock properties such as porosity, permeability and composition and their physical property such as elastic velocity, density and resistivity. On a related note, it is most advantageous to develop rock physics models to simultaneously explain both velocity and resistivity logs because while velocity is effected by both morphology and saturation of hydrate, resistivity is largely effected by saturation (Collett, 2001). Further, newer logging-while-drilling (LWD) directional resistivity tools are well suited for studying laminated hydrate morphology (Cook et al., 2012).

The LWD logs acquired during the GOM JIP Leg II included gamma-ray, density porosity, resistivity, acoustic velocity and caliper logs (Figure 2). Of the hydrate-bearing intervals interpreted based on high resistivity, the lower interval is considered as the sand reservoir (Figure 2). The Caliper log indicates several instances of borehole washouts within the sandy unit. Consequently, the porosity (from the bulk density log) is highly overestimated in the washout intervals. Lee and Collett (2012) suggested that porosities within the washout intervals can be replaced by porosities based on a sand-clay model developed by Kolterman and Gorelick (1995). These porosities are shown in track (c) of Figure 2 (red line) and used in our rock physics modeling. As Figure 2 suggests, the corrected porosity is in the same ballpark as the porosities of sandy intervals that were not washed out.

The resistivity data were collected using Schlumberger's GeoVISION tool. GeoVISION can measure four types of resistivity (the shallow, medium, deep and ring resistivity) with lateral depths-of-investigation being ~2.5, 8, 13 and 18cm, respectively (Schlumberger, 2007). The ring resistivity is often used for studying hydrate-bearing sediments because it has the finest vertical resolution for its depth of investigation (Malinverno et al., 2008). Another form of resistivity, known as propagation resistivity, was measured from the EcoScope tool (Collett et al., 2012). EcoScope also collects three types of resistivity logs (A16L, A28L and A40L). These resistivity measurements have a larger lateral depth of investigation (130-175cm) but a lower vertical resolution (Schlumberger, 2008). These propagation measurements are collected at three source-receiver spacing - A16L at 41cm, A28L at 71 cm, and A40L at 100cm. In hole GC955H the characteristic separation of the three kinds of propagation resistivity, which is often caused by invasion of drilling fluids, is not obvious (Cook et al., 2012). At another site, occupied in the same expedition, Alaminos Canyon Block 21 (AC21) the A40L propagation resistivity was used to study the hydrate-bearing sands to avoid the effect of borehole washout (Cook and Tost, 2014). In AC21, the propagation resistivity was higher than all GeoVISION resistivity logs because of the borehole washout.

However, in GC955, the ring resistivity is higher than the propagation resistivity (A40L) within the sand interval (Figure 3), indicating that the ring resistivity is not influenced by borehole washout.

The compressional wave velocity was measured using both SonicVISION and SonicScope tools. However, the SonicVISION velocities were consistently ~3% less than the SonicScope velocities in water-saturated sediments. Based on a comparison between synthetic seismogram generated from both SonicVISION and SonicScope velocities and coincident field data, Lee and Collett (2012) suggested that SonicScope velocities best represented the in-situ physical properties. Therefore, for our modeling we use the SonicScope compressional wave velocities.

The hydrate saturation ( $S_h$ ) can be estimated from resistivity log using Archie's saturation equation (Archie, 1942) as:

$$S_h = 1 - (R_0 / R_t)^{1/n} \quad (1)$$

Where  $R_t$  is the measured resistivity,  $n$  is an empirical exponent, and  $R_0$  is the water-saturated or background resistivity.  $R_0$ , in turn, can be expressed as following:

$$R_0 = \left[ \frac{\phi^m}{aR_w} \right]^{-1} \quad (2)$$

where  $R_w$  is the resistivity of pore water,  $a$  and  $m$  are Archie constants, and  $\phi$  is the porosity.

After obtaining the saturation from equations 1 and 2, morphology needs to be decided. Models for pore-filling, grain displacing and cementing hydrate in coarse-grained media has been well developed by Mavko et al. (2009). These models follow simple guidelines. The elastic moduli of drained rock matrix and pore fluid are independently estimated following which they are merged using a substitution scheme such as the Gassmann (1951) method. In the process a few assumptions are made. First, the pores are fully interconnected; second, the hydrate distribution is uniform; and third, the relaxation time is adequate. In the pore-filling morphology, hydrate is assumed to be suspended in the pore fluid. Thus, moduli of the sediment matrix and porosity remains unchanged while the effective bulk modulus of the composite pore fluid is the Reuss (1929) average of the water and hydrate bulk moduli. In load-bearing morphology, the original porosity is reduced and the bulk moduli of the solid frame is altered while the pore fluid modulus remains the same. In the cementation model, bulk moduli of solid frame rapidly increases even at low hydrate saturation.

Model for a laminated medium was proposed by Lee and Collett (2009) originally to account for fractured hydrate-bearing reservoir. This model is composed of two end-members: one is 100% water-saturated sediment matrix and the other is 100% gas hydrate-saturated void. While each of the end-members can remain isotropic, the laminated model creates a composite medium which is transverse isotropic (TI) media. Bulk modulus in TI media can be derived as follows. Let  $\eta_1$  and  $\eta_2$  be the volume fraction of the first and second end-members, respectively. The phase velocities of TI media could be computed using the following definition:

$$\langle G \rangle \equiv (\eta_1 G_1 + \eta_2 G_2)$$

$$\langle \frac{1}{G} \rangle \equiv (\eta_1 / G_1 + \eta_2 / G_2) \quad (3)$$

where G is any elastic constant. The compressional and shear wave velocities of TI media can be calculated from the following equations the Lamé constants  $\lambda$  and  $\mu$  :

$$A = \langle \frac{4\mu(\lambda + \mu)}{\lambda + 2\mu} \rangle + \langle \frac{1}{\lambda + 2\mu} \rangle^{-1} \langle \frac{1}{\lambda + 2\mu} \rangle^2$$

$$C = \langle \frac{1}{\lambda + 2\mu} \rangle^{-1}$$

$$F = \langle \frac{1}{\lambda + 2\mu} \rangle^{-1} \langle \frac{\lambda}{\lambda + 2\mu} \rangle$$

$$L = \langle \frac{1}{\mu} \rangle^{-1}$$

$$N = \langle \mu \rangle$$

$$\rho = \langle \rho \rangle$$

$$V_p = \left( \frac{A \sin^2 \varphi + C \cos^2 \varphi + L + Q}{2\rho} \right)^{1/2}$$

$$V_s^v = \left( \frac{A \sin^2 \varphi + C \cos^2 \varphi + L - Q}{2\rho} \right)^{1/2}$$

$$V_s^H = \left( \frac{N \sin^2 \varphi + L \cos^2 \varphi}{\rho} \right)^{1/2}$$

$$Q = \sqrt{[(A - L) \sin^2 \varphi - (C - L) \cos^2 \varphi]^2 + 4(F + L)^2 \sin^2 \varphi \cos^2 \varphi} \quad (4)$$

where  $\varphi$  is the angle between the wavefront normal and the vertical axis,  $V_p$  is the anisotropic compressional wave velocity,  $V_s^H$  is the horizontally polarized shear wave velocity, and  $V_s^V$  is the vertically polarized shear wave velocity (Lee and Collett, 2009). In the case of vertical and horizontal ray angles, the group velocities are the same as the phase velocities.

## Results:

### Saturation estimates from resistivity

Equations (1) and (2) are used to calculate the gas hydrate saturations from the ring resistivity and the propagation resistivity (A40L). The parameter takes 2 as proposed by Lee and Collett (2012). The Archie constants and are used in our modeling. The results are illustrated in track (b) of Figure 3. Three sublayers of concentrated gas hydrate occur in sands of Hole GC955H: the first is between 413.5 and 440.5 mbsf; the second is between 445 and 447 mbsf; the third is a thin bed near 449.5 mbsf (Cook et al., 2012). The first sublayer contains gas hydrate within sand with average gas hydrate saturations estimated at 66.2% from the ring resistivity and 56.8% from the propagation resistivity. The average gas hydrate saturations within the second sublayer are 47.8% estimated from ring resistivity and 27.8% from propagation resistivity, respectively. The third sublayer has average gas hydrate saturations of 47.6% estimated from the ring resistivity and 4.7% estimated from propagation resistivity.

### Saturation estimates from velocity

In the isotropic conditions, load-bearing and cementation morphology are assumed to model the velocity of gas hydrate-bearing sand sediment. Pore-filling morphology was abandoned because gas hydrate in this case does not affect the stiffness of the dry frame. The gas hydrate saturations estimated from velocity assuming isotropic models are shown in Figure 4a. The first sublayer contains gas hydrate within sand with average gas hydrate saturations estimated at 60.2% assuming load-bearing model and 12.2% assuming grain-cementing model. The average gas hydrate saturations within the second sublayer are 40.2% assuming load-bearing model and 6.7% assuming grain-cementing model, respectively. The third sublayer has average gas hydrate saturations of 42.3% assuming load-bearing model and 5.4% assuming grain-cementing model. In the laminated medium model, an incidence angle is used to represent wave propagation for a horizontal bed for a vertical borehole (Lee and Collett, 2009). The consolidation parameter is used the same as in Lee and Collett (2012). The gas hydrate saturation estimated from velocity assuming laminated medium model is shown in Figure 4b. The average saturations of the three sublayers are 67.5%, 47.1% and 46.5% respectively.



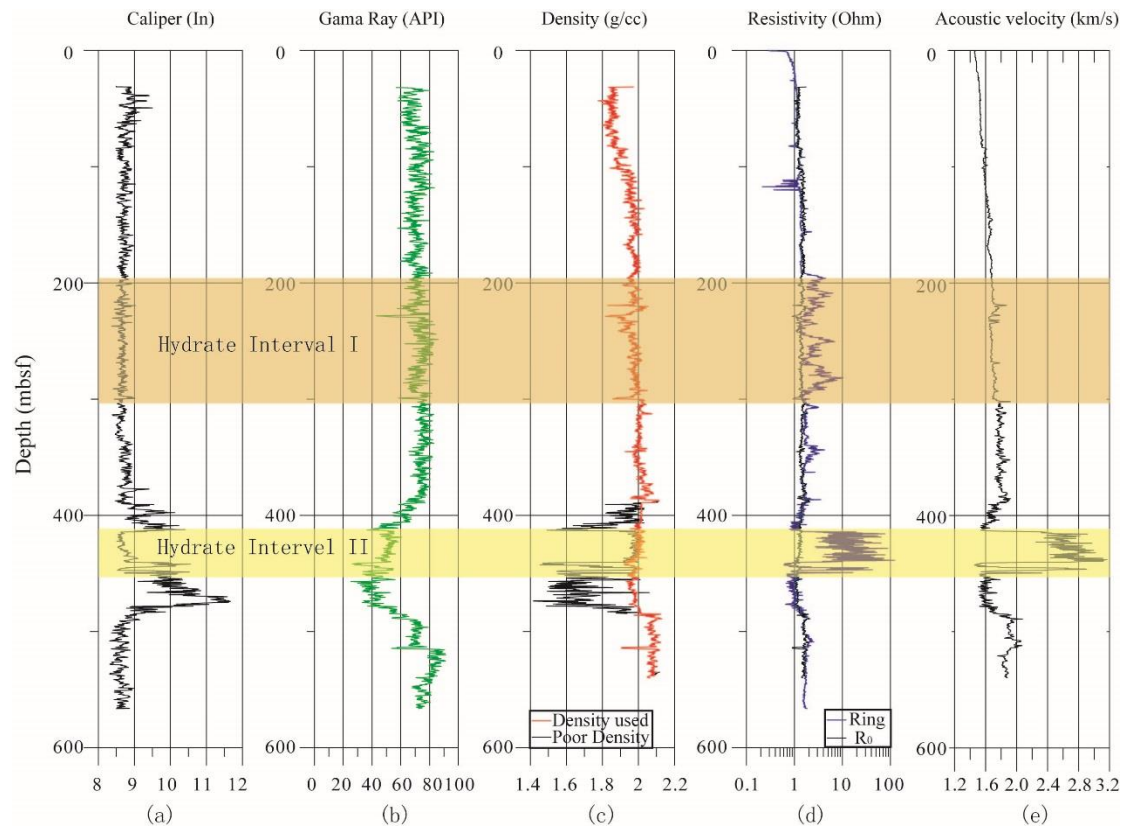


Figure 2. Geophysical well log measurement from hole GC955H. Two gas hydrate interval could be inferred from the logs with Hydrate Interval I occurring in clay-rich sediment at the shallow and Hydrate Interval II occurring in sand-prone sediment at the deep. Significant washout took place within the sands during drilling. The measured density is not reliable within the sand interval. The density used for saturation estimations is corrected using Kolterman and Gorelick (1995).

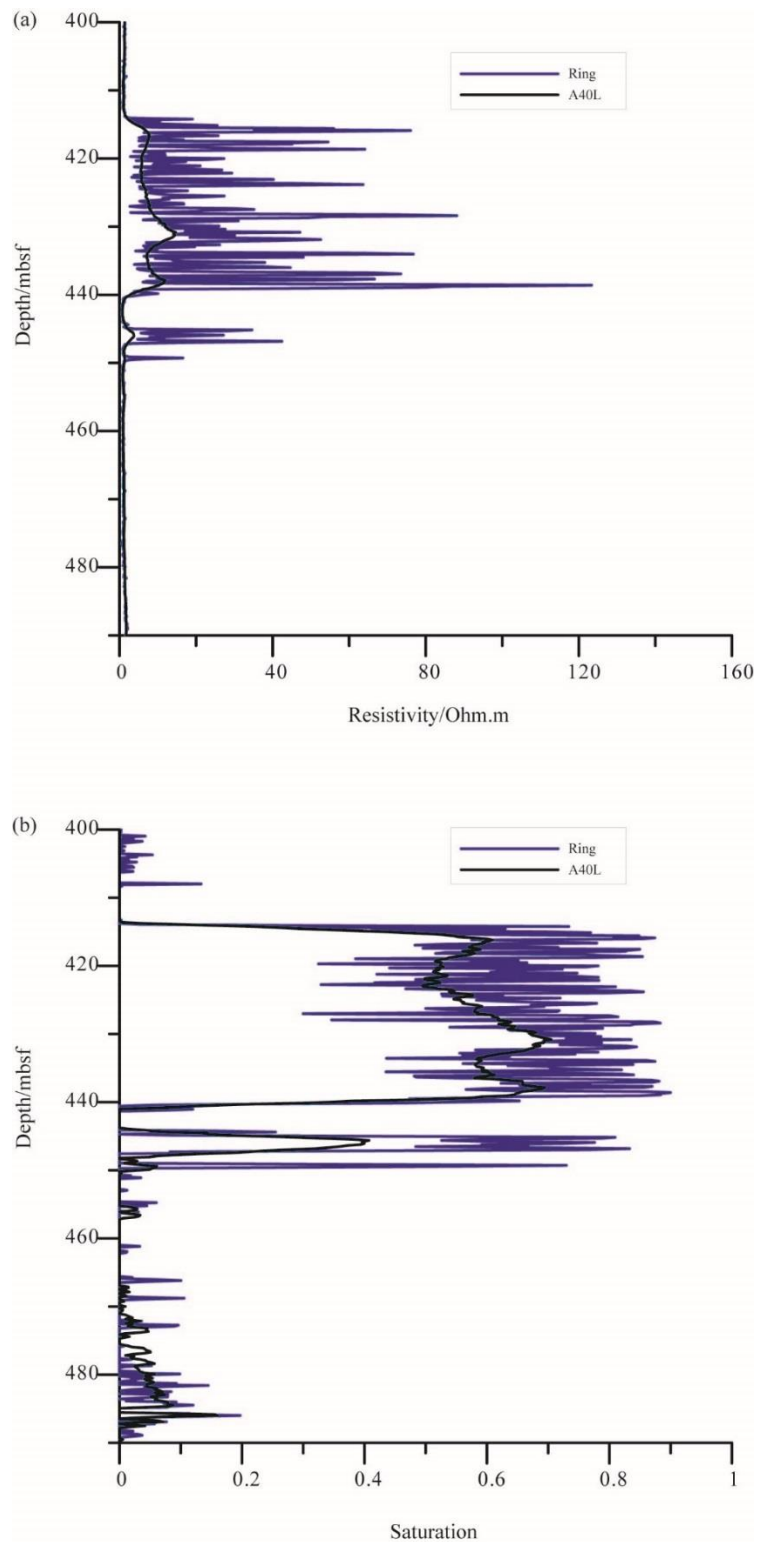


Figure 3. The resistivity logs and gas hydrate saturations estimated from resistivity using Archie's equation (1942). (a) The ring resistivity (blue line) and the propagation resistivity (A40L) (Black line). (b) The gas hydrate saturations estimated from the ring resistivity (blue line) and the propagation resistivity (red line).

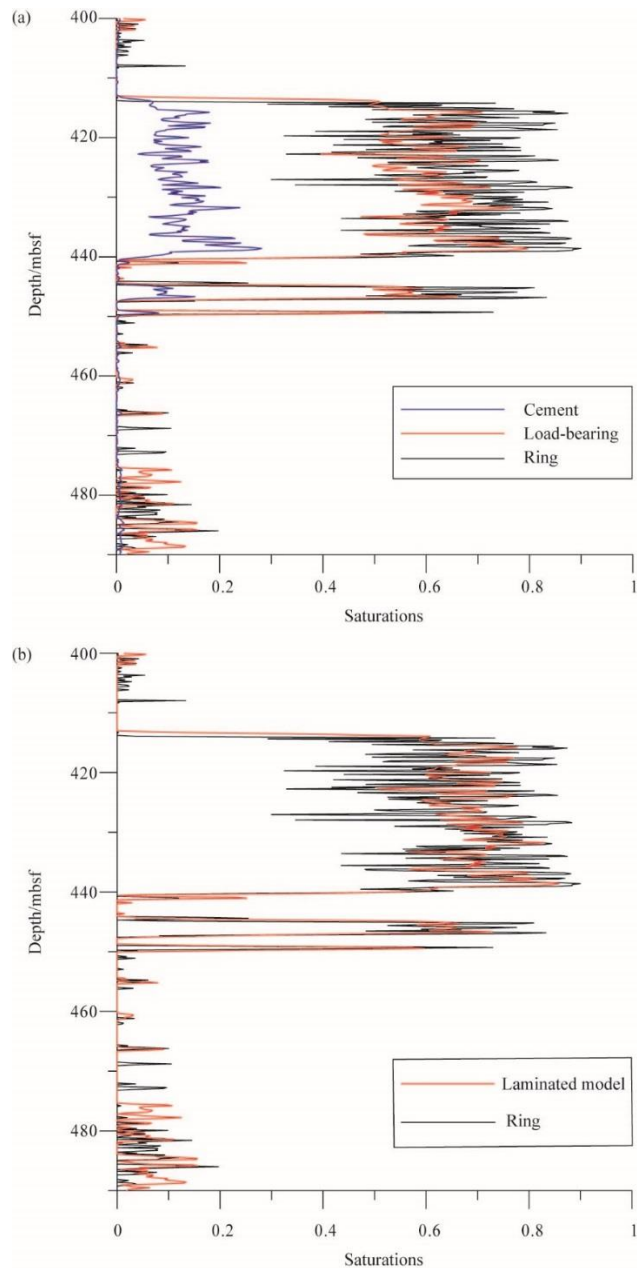


Figure 4. The gas hydrate saturations estimated from the velocity using different models. The black line represents the saturations estimated from the ring resistivity as reference. (a) The saturations are calculated from velocity assuming isotropic model. The blue line is the gas hydrate saturation using cementation model. The red line is the gas hydrate saturation using load-bearing model. The saturations using isotropic model are smaller than those estimated from the ring resistivity. (b) The red line is the gas hydrate saturations using laminated medium model. Even though the saturations from resistivity are pricklier than those from velocity, the averaged gas hydrate saturations within sublayers agree well with each other.

**Conclusions:**

(1) The presence of gas hydrate stiffens the stability of borehole wall in hole GC955H. Shallow sand sediments typically wash away during drilling because sand sediments lack the cohesion of clay-dominated sediments. When the gas hydrate saturation exceeds some critical value, gas hydrate bridges the neighboring grains of sediments, increases the stiffness of sediments and enhances the mechanical stability of borehole wall. Within the interval of gas hydrate-bearing sands, little or smaller borehole enlargements are observed compared to the interval of the hydrate-free sands in hole GC955H.

(2) Thin layers of gas hydrate occur within sands of hole GC955H. The gas hydrate saturations estimated from the ring resistivity and the propagation resistivity (A40L) varies with each other. The gas hydrate saturations estimated from velocity assuming isotropic model (load-bearing) and from the ring resistivity have a 6% discrepancy within the first sublayer of hydrate-bearing sands. Taken anisotropy into consideration, the gas hydrate saturations estimated from velocity using a laminated medium model is consistent with those estimated from the ring resistivity. Based on these saturation analysis, it's suggested that thin layers of gas hydrate occur within sands of hole GC955H.

**Milestone Status:**

Milestone	Description	Status	Schedule
Traveltime Inversion Model	The recipient shall compare the real and predicted reflection traveltimes from the final velocity model to be used for PSDM.	Done for CGGVeritas Datase and for the USGS dataset	Completed on target
Depth Migrated Image	The recipient shall compare structure and stratigraphy between the final depth image and images in literature and SSRs.	Done	Completed on target
Waveform velocity model	The recipient shall compare waveform inversion velocity and	Done	Completed On target

	sonic logs at well locations.		
Waveform attenuation model	The recipient shall compare real and synthetic simulated data.	Done	Completed On target
Rock physics model	The recipient shall compare predicted hydrate saturation at well locations with that available in the literature and methods of other DOE funded PIs, if available.	Ongoing	On target
Saturation map	The recipient shall compare consistency between hydrate distribution and structural/stratigraphic features interpreted in the study area.	Ongoing	On target

## References:

- Collett, T. S. (2001). A review of well-log analysis techniques used to assess gas-hydrate-bearing reservoirs. *Natural Gas Hydrates: Occurrence, Distribution, and Detection*, Geophysical Monographs, 124, 189-210.
- Collett, T. S., Lee, M. W., Zyrianova, M. V., Mrozewski, S. A., Guerin, G., Cook, A. E., and Goldberg, D. S. (2012). Gulf of Mexico Gas Hydrate Joint Industry Project Leg II logging-while-drilling data acquisition and analysis. *Marine and Petroleum Geology*, 34(1), 41-61.
- Cook, A. E., Anderson, B. I., Rasmus, J., Sun, K., Li, Q., Collett, T. S., and Goldberg, D. S. (2012). Electrical anisotropy of gas hydrate-bearing sand reservoirs in the Gulf of Mexico. *Marine and Petroleum Geology*, 34(1), 72-84.
- Koltermann, C. E., and Gorelick, S. M. (1995). Fractional packing model for hydraulic conductivity. *Water Resources Research*, 31(12), 3283-3297.
- Lee, M. W., and Collett, T. S. (2012). Pore-and fracture-filling Gas hydrate reservoirs in the Gulf of Mexico Gas hydrate Joint Industry Project leg II Green Canyon 955 H well. *Marine and Petroleum Geology*, 34(1), 62-71.
- Schlumberger (2007). GeoVISION Brochure: Resistivity imaging for productive drilling. [<http://www.slb.com/~media/Files/drilling/brochures/lwd/vision/geovision.pdf>.]
- Malinverno, A., Kastner, M., Torres, M. E., and Wortmann, U. G. (2008). Gas hydrate occurrence from pore water chlorinity and downhole logs in a transect across the northern Cascadia margin (Integrated Ocean Drilling Program Expedition 311). *Journal of Geophysical Research: Solid Earth* (1978–2012), 113(B8).
- Cook, A. E., and Tost, B. C. (2014). Geophysical signatures for low porosity can mimic natural gas hydrate: An example from Alaminos Canyon, Gulf of Mexico. *Journal of Geophysical Research: Solid Earth*, 119(10), 7458-7472.
- Gassmann, F. (1951), Elastic Waves Through A Packing Of Spheres, *Geophysics*, 16(4), 673-685.
- Mavko, G., T. Mukerji, and J. Dvorkin ( 2009), *The Rock Physics Handbook*, Second ed., Cambridge University Press, Cambridge, England.

Reuss, A. (1929). Berechnung der Fließgrenze von Mischkristallen auf Grund der Plastizitätsbedingung für Einkristalle. ZAMM - Journal of Applied Mathematics and Mechanics/Zeitschrift für Angewandte Mathematik und Mechanik, 9(1), 49-58.

## **National Energy Technology Laboratory**

626 Cochrans Mill Road  
P.O. Box 10940  
Pittsburgh, PA 15236-0940

3610 Collins Ferry Road  
P.O. Box 880  
Morgantown, WV 26507-0880

13131 Dairy Ashford Road, Suite 225  
Sugar Land, TX 77478

1450 Queen Avenue SW  
Albany, OR 97321-2198

Arctic Energy Office  
420 L Street, Suite 305  
Anchorage, AK 99501



Visit the NETL website at:

[www.netl.doe.gov](http://www.netl.doe.gov)